Steady-state ^{226}Ra/^{230}Th disequilibrium in mantle minerals: Implications for melt transport rates in island arcs[☆]

Maureen D. Feineman [a,b,*], Donald J. DePaolo [a,c]

[a] *Department of Earth and Planetary Science, University of California, Berkeley, CA 94720-4767, USA*
[b] *Institute for Geophysics and Planetary Physics, L-206, Lawrence Livermore National Laboratory, Livermore, CA 94550, USA*
[c] *Earth Sciences Division, MS 90R-1116, E.O. Lawrence Berkeley National Laboratory, Berkeley, CA 94720, USA*

Abstract

Measurements of the concentrations of the ^{238}U decay series isotopes (^{234}U, ^{230}Th, ^{226}Ra) have been used to estimate the rates at which magma is generated and transported in the mantle. The usual assumption is that solid mantle minerals are in radioactive equilibrium prior to melting. However, if one or more of the nuclides in the chain is strongly concentrated by a minor mineral, and if the diffusivity of that nuclide is large enough, steady-state radioactive disequilibrium can result in the solid phase. It can be inferred from available data that radium is strongly concentrated in minor hydroxyl-bearing mantle minerals (phlogopite and amphibole) relative to Th, and Ra diffusion in clinopyroxene is fast relative to the typical grain diameter at ca. 1100°C. Consequently, we show with simple analytical models that a steady-state Ra deficiency in clinopyroxene (cpx), accompanied by a complementary steady-state Ra excess in neighboring phlogopite (phlog) or amphibole (amph), is likely to be the normal situation in hydrous mantle peridotite with average clinopyroxene grain radii of ca. 1 mm. The steady state (^{226}Ra/^{230}Th) (parentheses indicating activity ratio) in the hydrous mineral is limited roughly by the mass ratio with clinopyroxene (i.e. cpx/phlog or cpx/amph) and could be as high as 10–100. The exceptionally high (^{226}Ra/^{230}Th) of some island arc lavas could therefore be a result of preferential contribution of phlogopite or amphibole during partial melting of hydrous mantle. This effect may ease time constraints for source-to-surface melt migration at island arcs. Incipient melting of hydrous minerals from channel walls during melt transport and/or late-stage incorporation of phlogopite or amphibole into arc magmas may also contribute to generating high (^{226}Ra/^{230}Th). Steady-state (^{226}Ra/^{230}Th) disequilibrium due to diffusive loss of ^{226}Ra from clinopyroxene is also important for melt/solid and fluid/solid partitioning, and must be incorporated into models relating isotopic disequilibrium to melt and fluid transport rates. Diffusive effects could be important for other U-series nuclides in some circumstances.
© 2003 Elsevier B.V. All rights reserved.

Keywords: Th-230/Ra-226; island arcs; diffusion; disequilibrium; phlogopite; amphibole

* Corresponding author. Tel.: +1-510-642-9116; Fax +1-510-642-9520.
  E-mail address: feineman@uclink4.berkeley.edu (M.D. Feineman).

1. Introduction

Measurements of the intermediate decay products of ^{238}U, such as ^{234}U, ^{230}Th, ^{226}Ra, have become an essential tool for understanding the generation and transport of magma in the Earth (e.g. [1–4]). The relatively short-lived nuclide ^{226}Ra ($t_{1/2} = \sim 1.6$ ka) is particularly interesting in that, if present in excess in lavas, it implies that melting and magma transport in the mantle take place on a time scale of less than a few thousand years. Although melt transport processes may extend the duration of disequilibrium [3], the degree of ^{226}Ra excess is limited by the mineral/melt partition coefficient. Early alpha- and gamma-spectroscopic studies of arc lavas [5–7], and more recently improved mass spectrometric techniques for ^{226}Ra measurement ([8–16], etc.) have prompted the collection of a large body of data over the past several years, from which interesting and puzzling features have emerged. In particular, observed excesses of ^{226}Ra relative to ^{230}Th in igneous rocks are typically larger than expected based on mineral/melt partition coefficients for Ra and Th. The largest excesses have been observed in island arc lavas [7–8], and lesser but notable excesses have been observed in mid-ocean ridge basalts (MORB) [9–10]. Ocean island lavas generally have smaller ^{226}Ra excesses more consistent with ^{230}Th excesses [11] (Fig. 1). The
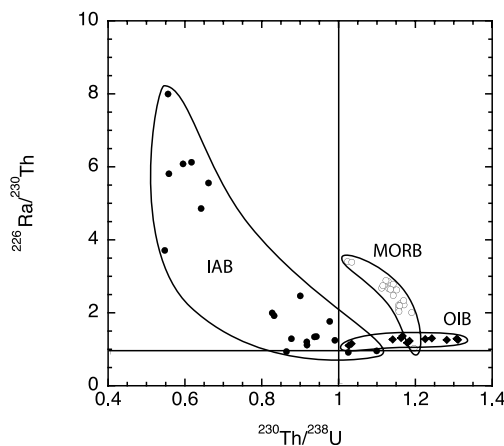
large excesses of ^{226}Ra in island arc lavas have been interpreted as an indication that magma is transported from subduction zone depths (ca. 100 km) to the surface in only a few hundred years [8,12]. Recently, however, the usefulness of U-series isochrons for determining time scales of melt generation and migration at subduction zones has been called into question [18]. Attempts to explain the decoupling of Ra isotopes from those of Th at arcs involve interaction of the mantle with slab-derived aqueous [8,12] or carbonatitic [16] fluids, and are based on the inferred geochemical behavior of Ra. Direct experimental investigation of the behavior of Ra has proven difficult due to its high radioactivity, and in situ measurement of ^{226}Ra is difficult due to its low concentration (~ 1–10 fg/g) in most naturally occurring minerals. However, since radium is chemically similar to barium, it is thought to be fluid-soluble in contrast to the extremely insoluble Th. Consequently, in subduction zones, where fluids are abundant, there is a greater likelihood of producing more extreme Ra/Th fractionation than in other magma generation settings.

In this paper we investigate a previously unrecognized mechanism for producing large Ra/Th fractionation in island arc magmas. The effect stems from competition between radioactive and chemical equilibrium. When a crystal grows in chemical (dynamic) equilibrium with its surroundings, trace elements, including parent and daughter nuclides, are incorporated into the crystal according to their equilibrium partition coefficients (for the purposes of this paper, K is used instead of the conventional D to denote the partition coefficient in order to avoid confusion with the diffusion coefficient). The relationship between the parent-to-daughter elemental concentration ratios in two mineral phases at chemical equilibrium is given by:

$$\frac{[p]_i}{[d]_i} = \frac{[p]_j}{[d]_j} \cdot \frac{K_p^{i/j}}{K_d^{i/j}} \tag{1}$$

where the square brackets denote concentration, i is the crystalline phase of interest, j is any phase (liquid or solid) in equilibrium with i, and K is the equilibrium partition coefficient between the two phases.

Fig. 1. ($^{226}Ra/^{230}Th$) vs. ($^{230}Th/^{238}U$) for basalts. IAB data from [8,12,14,17]; MORB data from [9,10]; and OIB data from [11].

If the two elements are part of the same uranium decay series, however, one being the parent of the other, the ratio of parent-to-daughter at radioactive or secular equilibrium would be the same in both mineral phases, and given by:

$$\frac{[p]_i}{[d]_i} = \frac{\lambda_d}{\lambda_p} \qquad (2)$$

where λ is the radioactive decay constant. The expected parent/daughter ratios dictated by Eqs. 1 and 2 can differ by several orders of magnitude. If diffusive exchange between mineral phases is very slow, or negligible, each mineral grain will be a 'closed system' and Eq. 2 will apply to all mineral grains. However, if diffusive exchange between mineral grains is fast relative to the radioactive mean life of the parent nuclide, Eq. 1 will apply. In general, natural minerals have parent/daughter ratios somewhere between the values specified by Eqs. 1 and 2. The precise values are determined by the diffusion coefficients of the elements involved in the minerals of interest, the radioactive mean life of the parent, and the size of the mineral grains.

Strong fractionation of Ra from Th is expected between some solid phases in the Earth's mantle. In particular, hydroxyl-bearing minerals, such as phlogopite and amphibole, strongly concentrate Ba (and by inference Ra) in preference to Th. Hence, in solid mantle rocks at high temperatures, there is a tendency for ^{226}Ra to accumulate in hydrous minerals, even though its parent isotope, ^{230}Th, is housed mainly in clinopyroxene. The accumulation of ^{226}Ra in the hydrous minerals is mainly limited by the diffusivity of Ra in clinopyroxene, and can result in both clinopyroxene and the hydrous minerals maintaining significant steady-state radioactive disequilibrium. The predicted pronounced radioactive disequilibrium in the solid state has not heretofore been recognized or incorporated into magma generation models. Solid-state disequilibrium may provide an explanation for certain large observed ^{226}Ra excesses, may ease the time restrictions for melt generation and transport for island arc lavas, and may have implications for the interpretation of ^{226}Ra excesses in other settings as well.

2. Origins of phlogopite- and amphibole-bearing peridotite

Phlogopite and amphibole form when aqueous fluid or hydrous melt interacts with normal mantle peridotite. Interactions of this sort are commonly associated with subduction zone processes. As the oceanic plate is subducted and subjected to increasing pressures and temperatures, aqueous fluids and/or hydrous melts are driven out of the slab. The fluids or melts then migrate into the overlying mantle wedge, where they may induce melting directly, or may react with the mantle to form new, hydrous mineral-bearing assemblages [19]. Wyllie and Sekine [20] proposed that a hydrous silicate melt leaving the slab and migrating into the overlying mantle wedge will react with peridotite to form phlogopite ± enstatite ± quartz, expelling aqueous fluid in the process. A beautiful example of phlogopite- and amphibole-bearing peridotite is found at the Finero peridotite massif in the Ivrea–Verbano zone in northern Italy [21]. Phlogopite- and amphibole-bearing peridotite nodules are found in lavas throughout the world, including Siberia and Mongolia [22,23], Eifel, Germany [23], Victoria, Australia [24], and Kerguelen [25].

3. Trace element partitioning in phlogopite, amphibole, and clinopyroxene

Barium is similar to Ra in charge (2+) and ionic radius (1.61 Å vs. 1.70 Å in 12-coordination [26]), and therefore serves as a model for predicting Ra chemical behavior. Although accounting for the effect of the difference in radii between Ra and Ba on the partition coefficients for these elements is significant in certain scenarios [13], the correction is small in relation to the several orders of magnitude difference between Ba and Th partitioning, and is smallest when the trace elements substitute for K (1.64 Å in 12-coordination), as is the case for phlogopite. Available experimental data (Fig. 2) suggest that Ba is strongly concentrated in phlogopite and amphibole relative to clinopyroxene (average $\sim 30\,000\times$ and $\sim 600\times$, respectively, due to the large A-sites in micas and

amphiboles). Thorium, by contrast, has a partition coefficient of ~ 1 between the hydrous phases and clinopyroxene. In selecting data for Fig. 2, preference was given to experimental data from a single experiment. The remaining experimental data are ratios of mineral/fluid or mineral/melt partition coefficients (e.g. phlog/fluid:cpx/fluid, phlog/melt:cpx/melt) determined in separate experiments. In the latter case, fluids and melts with similar compositions were chosen for constructing the ratios. The ratios determined from experimental data are consistent with in situ and mineral separate analyses of minerals in natural rocks. Many of the natural rock analyses yield amph/cpx partition coefficients for Ba that are considerably higher than the experimental data, suggesting that the K_{Ba} (and resultant K_{Ra}) used in our amphibole calculations may be lower boundary values.

The experimental data on mineral/melt and mineral/fluid partitioning for Ba^{2+} and other cations (Sr^{2+}, Ca^{2+}, Na^+, K^+, Rb^+) can be used to make quantitative estimates of Ra^{2+} partitioning using the elastic strain model of Blundy and Wood [32,33]. The model is an extension of the Brice equation [34], which describes strain on a lattice site due to elemental substitution as a function of the Young's modulus (E) and the radius of the substituting cation (r_i) relative to the optimum (unstrained) ionic radius (r_o). The partition coefficient of element i (K_i), defined as the ratio of concentration in the mineral to concentration in the fluid phase, is predicted by:

$$K_i = K_o \exp\left[\frac{-4\pi E N_A \left[\frac{r_o}{2}(r_i - r_o)^2 + \frac{1}{3}(r_i - r_o)^3\right]}{RT}\right] \quad (3)$$

where N_A is Avogadro's number, R is the gas constant, and T is temperature in Kelvin. K_o is the 'strain-compensated partition coefficient' that describes the strain-free substitution of a hypothetical cation whose ionic radius is equal to r_o. K_o, r_o, and E are determined by fitting Eq. 3 to the partitioning data from an isovalent set of elements. Table 1 lists calculated Ra and measured Ba and Th partition coefficients and model parameters for minerals in equilibrium with melt
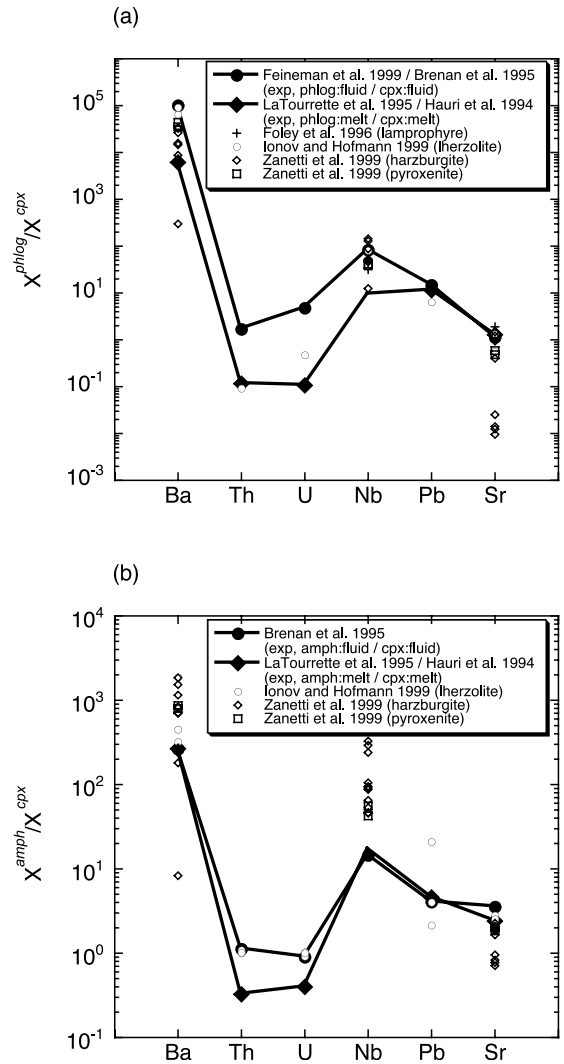

Fig. 2. (a) Phlogopite/clinopyroxene and (b) amphibole/clinopyroxene partitioning of trace elements from experimental data and natural rocks. Large closed symbols connected by bold lines represent experimental data, which are given prevalence in our calculations; circles are minerals in equilibrium with aqueous fluid (phlog: [27], amph and cpx: [28]), diamonds are minerals in equilibrium with melt (phlog and amph: [29], cpx: [30]). Small open symbols represent in situ or mineral separate analyses of phlog or amph and cpx coexisting in natural rocks; circles are lherzolite xenoliths from Mongolia [22], diamonds are harzburgite and squares are pyroxenite from the Finero peridotite massif [21], and crosses are a lamprophyre from Newfoundland [31].

or fluid. All r_o, E_0, and K_{Ra}/K_{Ba} are in agreement with the values presented by Blundy and Wood [35]. The average phlog/cpx ratio for Ra is $\sim 5 \times 10^5$, and the average amph/cpx is ~ 500. These values for K_{Ra} between clinopyroxene and the hydrous minerals are similar in magnitude to the measured K_{Ba} values shown in Fig. 2. The existing data and models clearly indicate that the equilibrium Ra/Th ratio of both phlogopite and amphibole should be far higher than that of coexisting clinopyroxene.

4. Diffusion of Ra and Th in clinopyroxene

Diffusion data for Th and U [36], in conjunction with elastic strain modeling [37], provide a means for comparing diffusion coefficients for Ra, Th, and U [38]. The resulting calculated diffusion coefficients for clinopyroxene are shown in Fig. 3. The diffusivity of Ra (D_{Ra}) is apparently about 1000 times greater than either D_U or D_{Th}, and strongly temperature-dependent. Whenever the diffusion path length (i.e. grain radius) is less than or equal to $(D_{Ra}/\lambda_{Ra})^{1/2}$, a large fraction of the radiogenic ^{226}Ra will be able to leave the crystal before it decays to ^{222}Rn. At lower temperatures ($\sim 1000°C$), only the rim of the clinopyrox-
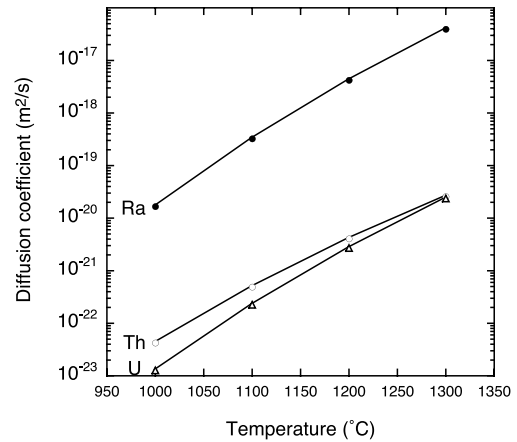

Fig. 3. Diffusion coefficients for Ra, Th, and U in diopside. Data for Th and U from [36], data for Ra from [38], predicted using elastic strain model of [37].

ene grain will lose ^{226}Ra by diffusion, whereas at higher temperatures ($\sim 1250°C$), an entire 2 mm radius clinopyroxene grain will be in disequilibrium due to diffusive Ra loss. At temperatures between 1100 and 1200°C, the calculation indicates that most of the radiogenic ^{226}Ra will diffuse out of clinopyroxene crystals with diameters in the range 0.5–2 mm. For both Th and U, the diffusion is too slow for any significant amount of migration on the time scale of Ra decay.

Table 1
Experimental Ba, Th partition coefficients and calculated Ra partition coefficients with parameters for elastic strain model

	K_{Ba}	K_{Th}	K_{Ra}	K_{Ra}/K_{Ba}	$r_o{}^a$ (Å)	K_o	E (GPa)
Phlog/melt[b]	3.68	1.4×10^{-3}	2.82	0.77	1.64	3.92	165
Phlog/fluid[c]	88.7	9.28	71.1	0.80	1.64	95.1	124
Amph/melt[b]	0.16	3.9×10^{-3}	1.49×10^{-2}	0.09	1.51	0.42	170
Amph/fluid[d]	0.51	0.93	3.89×10^{-2}	0.08	1.51	1.30	153
Cpx/melt[e]	6×10^{-4}	1.2×10^{-2}	3.13×10^{-5}	0.05	1.05	1.16	157
Cpx/fluid[d]	1.94×10^{-3}	0.83–5.5	8.72×10^{-5}	0.05	1.05	4.85	114

[a] r_o assumed to be constant for a given lattice site.
[b] All model parameters (r_o, K_o, E) from [29], assuming substitution on A-site (12-coordinated). For amphibole, 85% of the Sr was assumed to reside on the A-site, after [35].
[c] K_o and E calculated by linear regression of experimentally determined partition coefficients for divalent elements (Ba and Sr) [27], assuming substitution on A-site.
[d] K_o and E calculated by linear regression of experimentally determined partition coefficients for divalent elements (Ba and Sr) from [28]. For amphibole, 50% of the Sr was assumed to reside on the A-site in order to obtain reasonable values for E from the regression.
[e] r_o from [32], K_o and E calculated by linear regression of experimentally determined partition coefficients for divalent elements from [30], assuming substitution on M2-site (8-coordinated).

5. Diffusion–decay model

The primary issue for this problem is determining the boundary conditions for the diffusion calculation. In general, phlogopite grains present in hydrous peridotite are not in direct contact with clinopyroxene grains. Any Ra that can diffuse out of clinopyroxene grains must migrate along grain boundaries and then diffuse into phlogopite grains. The problem is simplified if it is assumed that the time scale for grain boundary diffusion is very short in comparison to intragranular diffusion. This should be a good approximation, as typically grain boundary diffusion is roughly 10^4 times faster than intragranular diffusion [39]. As a further approximation, we assume that no concentration gradients of Ra exist in phlogopite grains. This approximation should also be adequate because the phlogopite grains are likely to be significantly smaller than the average clinopyroxene grains, and the diffusivity of Ra (by analogy with Sr and presumably other large alkaline earth elements) in phlogopite is $\sim 10^2$–10^4 times greater than in clinopyroxene [40,41]. Consequently, the time scale for diffusive homogenization of phlogopite grains (a^2/D, where a is the grain dimension) is likely to be 100–1000 times shorter than that for clinopyroxene. Hence for the model, the overall assumption is that any Ra that diffuses out through the surface of a clinopyroxene grain into the intergranular medium is instantaneously added to a homogeneous nearby phlogopite grain. This assumption reduces the problem to one of calculating the diffusion of Ra in clinopyroxene, and conserving Ra atoms in the system that includes the clinopyroxene plus phlogopite.

The concentration of Ra at the surface of the clinopyroxene grains is assumed to be such that the clinopyroxene grain surface is always in equilibrium with phlogopite (as well as with the surfaces of all other grains in the rock) with respect to the concentrations of Ra and Th. Assuming that the radius of the clinopyroxene grains is 'a', then we specify that $C_{226}^{cpx}(a) = C_{226}^{phlog}/K_{Ra}^{phlog/cpx}$, where C_n^i is the concentration of nuclide n in phase i, and $K_{Ra}^{phlog/cpx}$ is the equilibrium partition coefficient of Ra between phlogopite and clinopyroxene ($K_{Ra}^{phlog/cpx} = $[Ra]$_{phlog}/$[Ra]$_{cpx}$ at chemical equilibrium). Finally, we assume that diffusion in clinopyroxene is isotropic [42], such that a spherical grain will have a concentration gradient of zero at the center. A schematic profile of ^{226}Ra concentration from a clinopyroxene grain center, including an adjacent phlogopite grain, is shown in Fig. 4.

The concentration of ^{226}Ra in clinopyroxene is given by Fick's second law modified to account for radioactive ingrowth and decay. We present here the equations for both spherical clinopyroxene grains of radius a, as well as a simpler model of the clinopyroxene grains as infinite slabs of half-thickness a. In spherical coordinates the equation is:

$$\frac{\partial C_{226}^{cpx}}{\partial t} = D_{Ra}\left(\frac{\partial^2 C_{226}^{cpx}}{\partial r^2} + \frac{2}{r}\frac{\partial C_{226}^{cpx}}{\partial r}\right) +$$

$$\lambda_{230} C_{230}^{cpx} - \lambda_{226} C_{226}^{cpx} \tag{4a}$$

For the slab model, the equation is:

$$\frac{\partial C_{226}^{cpx}}{\partial t} = D_{Ra}\left(\frac{\partial^2 C_{226}^{cpx}}{\partial x^2}\right) + \lambda_{230} C_{230}^{cpx} - \lambda_{226} C_{226}^{cpx} \tag{4b}$$

where we have replaced the radial coordinate 'r' with 'x' in the second equation to indicate the one-dimensional nature of the second model. In these equations all of the concentrations are functions of time and position; and $C_n^{cpx}(r,t)$ (or $C_n^{cpx}(x,t)$) is the concentration of nuclide n in the clinopyroxene at a radius r (distance x) from the grain center at time t, D_{Ra} is the diffusion coefficient for Ra in clinopyroxene (a function of temperature), and λ_n is the decay constant of nuclide n. The boundary conditions used in the solution of Eq. 4a,b are:

$$\text{at } r = 0, \ \frac{\partial C_{226}^{cpx}}{\partial r} = 0 \tag{5}$$

$$\text{at } r = a, \ C_{226}^{cpx} = \frac{C_{226}^{phlog}}{K_{Ra}^{phlog/cpx}} \tag{6}$$

where r is the distance from the center of the clinopyroxene grain (i.e. $r = a$ represents the grain boundary). Substituting x for r in Eqs. 5 and 6 gives the boundary conditions for the slab model. In both models it is assumed that C_{230}^{cpx} is uniform throughout the clinopyroxene grains.
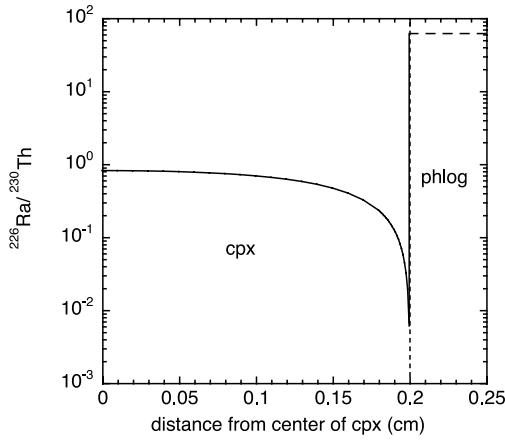
Fig. 4. Calculated (^{226}Ra/^{230}Th) profile through clinopyroxene and neighboring phlogopite at 1200°C. The clinopyroxene grain radius is 0.2 cm and the mass ratio of clinopyroxene to phlogopite (M^{cpx}/M^{phlog}) is 100. The activity ratio in the phlogopite is determined by the activity ratio in clinopyroxene at the grain boundary and the equilibrium partition coefficients K_{Ra} and K_{Th}, given the boundary condition $C^{phlog} = C^{cpx} K^{phlog/cpx}$ at $r = a$. Phlogopite thickness is not shown to scale.

The concentration of ^{226}Ra in the hydrous phase is determined by the flux of ^{226}Ra out of clinopyroxene, the relative masses of clinopyroxene and phlogopite, the decay of ^{226}Ra, and the production of ^{226}Ra by decay of ^{230}Th in phlogopite. The mass balance equation for the spherical clinopyroxene grain, including radioactive ingrowth and decay in phlogopite, is given by:

$$\rho^{phlog} V^{phlog} \frac{\partial C_{226}^{phlog}}{\partial t} = -\rho^{cpx} 4\pi a^2 D_{Ra} \left(\frac{\partial C_{226}^{cpx}}{\partial r} \right)_{r=a}$$

$$-\rho^{phlog} V^{phlog} \lambda_{226} C_{226}^{phlog} + \rho^{phlog} V^{phlog} \lambda_{230} C_{230}^{phlog}$$

where ρ^i is the density of phase i and V^{phlog} is the volume of phlogopite. This equation can also be written in the form:

$$\frac{\partial C_{226}^{phlog}}{\partial t} = -\frac{M^{cpx}}{M^{phlog}} \frac{3D_{Ra}}{a} \left(\frac{\partial C_{226}^{cpx}}{\partial r} \right)_{r=a}$$

$$-\lambda_{226} C_{226}^{phlog} + \lambda_{230} C_{230}^{phlog} \qquad (7a)$$

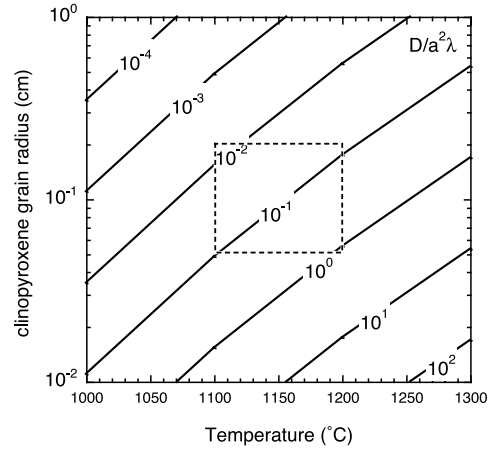where M^{cpx} and M^{phlog} are the masses of clinopy-

Fig. 5. Dimensionless diffusion variable $D/(a^2\lambda)$. For common upper mantle temperatures and clinopyroxene grain radii (i.e. 1100–1200°C and 0.05–0.2 cm), indicated by the dashed box, the value of this variable will be between ~ 0.01 and 1.

roxene and phlogopite, respectively (per unit volume of rock). The equation for the slab geometry is:

$$\frac{\partial C_{226}^{phlog}}{\partial t} = -\frac{M^{cpx}}{M_{phlog}} \frac{D_{Ra}}{a} \left(\frac{\partial C_{226}^{cpx}}{\partial x} \right)_{x=a}$$

$$-\lambda_{226} C_{226}^{phlog} + \lambda_{230} C_{230}^{phlog} \qquad (7b)$$

In both Eqs. 4a,b and 7a,b, time dependence is of little relevance to the model. Since the system approaches steady state in a time period of a few mean lives of ^{226}Ra ($1/\lambda_{226}$), which is several thousand years and hence geologically short, it is a good assumption that mantle rocks will normally be at steady state prior to the onset of melting. If the system has not yet come to steady state, the activity ratio in the hydrous phase will be higher than that predicted by the steady-state model, because it will be closer to the dynamic equilibrium ratio (as defined by Eq. 1). Comparison of Eqs. 7a and 7b shows that the essential difference between the spherical grain model and the slab model for clinopyroxene is that for the spherical grain model, clinopyroxene loses more of its Ra by diffusion for the same characteristic grain dimension a.

Solutions to the simultaneous Eqs. 4a,b and

7a,b are detailed in the Appendix[1]. The expression for the steady-state radium activity ratio in the phlogopite is:

$$R_{226}^{phlog} =$$

$$\frac{1 + \frac{3M^{cpx}}{M^{phlog}}\left(\frac{D_{Ra}}{a^2\lambda_{226}}\right)^{1/2}\frac{1}{K_{Th}^{phlog/cpx}}\coth\left(\frac{a^2\lambda_{226}}{D_{Ra}}\right)^{1/2} - \frac{3M^{cpx}}{M^{phlog}}\frac{D_{Ra}}{a^2\lambda_{226}}\frac{1}{K_{Th}^{phlog/cpx}}}{1 + \frac{3M^{cpx}}{M^{phlog}}\left(\frac{D_{Ra}}{a^2\lambda_{226}}\right)^{1/2}\frac{1}{K_{Ra}^{phlog/cpx}}\coth\left(\frac{a^2\lambda_{226}}{D_{Ra}}\right)^{1/2} - \frac{3M^{cpx}}{M_{phlog}}\frac{D_{Ra}}{a^2\lambda_{226}}\frac{1}{K_{Ra}^{phlog/cpx}}} \quad (8a)$$

or, for the slab geometry:

$$R_{226}^{phlog} =$$

$$\frac{1 + \frac{M^{cpx}}{M^{phlog}}\left(\frac{D_{Ra}}{a^2\lambda_{226}}\right)^{1/2}\frac{1}{K_{Th}^{phlog/cpx}}\tanh\left(\frac{a^2\lambda_{226}}{D_{Ra}}\right)^{1/2}}{1 + \frac{M^{cpx}}{M^{phlog}}\left(\frac{D_{Ra}}{a^2\lambda_{226}}\right)^{1/2}\frac{1}{K_{Ra}^{phlog/cpx}}\tanh\left(\frac{a^2\lambda_{226}}{D_{Ra}}\right)^{1/2}} \quad (8b)$$

Eq. 8a,b shows the dependence of the resulting activity ratio ($R_{226} = A_{226}/A_{230}$, where A denotes activity) on the mass ratio of clinopyroxene to phlogopite (M^{cpx}/M^{phlog}), the partition coefficients $K_{Th}^{phlog/cpx}$ and $K_{Ra}^{phlog/cpx}$, and the dimensionless diffusion parameter $D_{Ra}/(a^2\lambda_{226})$. The dimensionless diffusion parameter is a measure of the efficiency of ^{226}Ra redistribution, which increases with temperature (i.e. D_{Ra}) and decreases with clinopyroxene grain size. Values of $D_{Ra}/(a^2\lambda_{226})$ for expected ranges of temperature and grain size in the mantle are shown in Fig. 5. The profile of R_{226} in clinopyroxene is given by:

$$R_{226}^{cpx}(r) =$$
$$1 + \left(\frac{K_{Th}^{phlog/cpx}}{K_{Ra}^{phlog/cpx}}R_{226}^{phlog} - 1\right)\frac{a\sinh\left(\frac{r^2\lambda_{226}}{D_{Ra}}\right)^{1/2}}{r\sinh\left(\frac{a^2\lambda_{226}}{D_{Ra}}\right)^{1/2}} \quad (9a)$$

or, for the slab model:

$$R_{226}^{cpx}(x) =$$
$$1 + \left(\frac{K_{Th}^{phlog/cpx}}{K_{Ra}^{phlog/cpx}}R_{226}^{phlog} - 1\right)\frac{\cosh\left(\frac{x^2\lambda_{226}}{D_{Ra}}\right)^{1/2}}{\cosh\left(\frac{a^2\lambda_{226}}{D_{Ra}}\right)^{1/2}} \quad (9b)$$

The calculated activity ratios for both phlogopite and clinopyroxene are plotted in Fig. 6, for

---

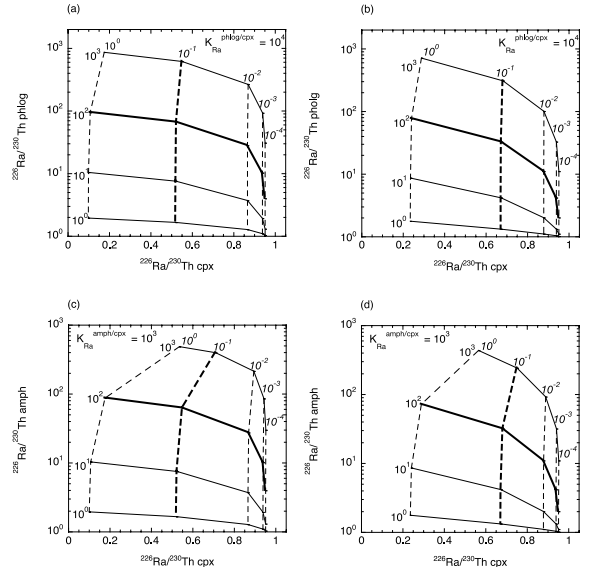[1] See online version of this article.

Fig. 6. ($^{226}Ra/^{230}Th$) in phlogopite and amphibole vs. clinopyroxene. Solid lines represent M^{cpx}/M^{phlog}, dashed lines represent $D/(a^2\lambda)$. Heavy lines denote probable mantle conditions ($M^{cpx}/M^{phlog} = 100$, $D/(a^2\lambda) = 0.1$). (a) Spherical model for phlogopite. (b) Slab model for phlogopite. (c) Spherical model for amphibole. (d) Slab model for amphibole.

different values of M^{cpx}/M^{phlog} and the dimensionless diffusion parameter. When M^{cpx}/M^{phlog} is large, the activity ratio in the phlogopite increases because the ^{226}Ra generated in the clinopyroxene is distributed throughout a smaller mass of phlogopite. The dimensionless diffusion parameter determines the total flux of ^{226}Ra between clinopyroxene and phlogopite, and consequently affects the activity ratios in both phases. Also shown are the activity ratios for amphibole and clinopyroxene, demonstrating the dependence of $^{226}Ra/$ ^{230}Th on K_{Ra}. Because the value of $K_{Ra}^{phlog/cpx}$ is so large, the depletion of ^{226}Ra in clinopyroxene is quite pronounced regardless of the amount of phlogopite present in the rock (also shown in Fig. 4). When $K_{Ra}^{amph/cpx}$, which is somewhat smaller than $K_{Ra}^{phlog/cpx}$, is substituted into Eqs. 8a,b and 9a,b, ^{226}Ra depletion in clinopyroxene is variable and dependent on M^{cpx}/M^{amph}. When the amount of amphibole is small, the clinopyroxene loses less of its ^{226}Ra prior to decay, bringing the activity ratio in the clinopyroxene closer to unity.

6. Melt and fluid phases in the mantle

The model can also be applied to a liquid phase generated by partial melting of a mantle mineral assemblage containing clinopyroxene with or without hydrous minerals. Clinopyroxene, which is the primary mantle mineral repository for Th, discriminates between Ra (or Ba) and Th [28,30]. Partial melting of peridotite (lherzolite) in the presence of residual clinopyroxene produces a silicate liquid, which should have (at equilibrium) Ra/Th that is somewhat elevated with respect to the solids by a factor that depends on the melt fraction (e.g. [3,4,11]). However, because both Ra and Th are very incompatible in clinopyroxene with respect to melt, the fractionation effect is minimized.

Eq. 8a,b above can be applied to the melt phase by substituting $K_{Th,Ra}^{melt/cpx}$ for $K_{Th,Ra}^{phlog/cpx}$, if it is assumed that the melt phase remains in contact with the solid for a time period exceeding a few mean lives of ^{226}Ra. Steady percolation of melt through solid will also produce the result described by Eq. 8a,b. The steady-state ($^{226}Ra/^{230}Th$) of melts and fluids is shown in Fig. 7 as a function of the mass ratio of melt or fluid to clinopyroxene. For melts, the activity ratio is elevated by less than a factor of 2 for melt fractions 100 times smaller than the clinopyroxene abundance. Many authors have investigated in detail the generation of U-series disequilibria in magmas by melting and transport processes, equilibrium and disequilibrium melting, porous and channelized flow, etc. [3,4,11,18,43–45]. Although the U-series systematics of MORB and ocean island basalts (OIB) can be satisfactorily explained by melting and transport phenomena, it has proven difficult to match the high ($^{226}Ra/^{230}Th$) in arc lavas without the incorporation of an additional component.

For an aqueous fluid the effect of discrimination by clinopyroxene is much stronger than for a melt (Fig. 7b). A fluid trapped in isolated pockets at grain boundaries due to incomplete wetting or percolating through lherzolite under steady conditions can achieve, and maintain during transport, ($^{226}Ra/^{230}Th$) in excess of 100 due to the preferential diffusion of ^{226}Ra out of clinopyroxene. When high ($^{226}Ra/^{230}Th$) fluids migrate into
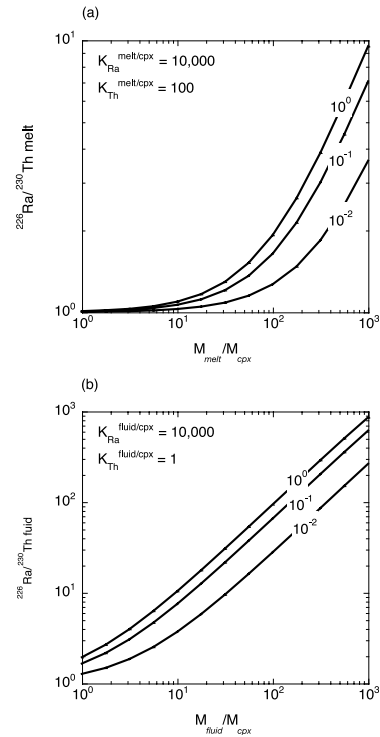

Fig. 7. ($^{226}Ra/^{230}Th$) in melt or aqueous fluid in equilibrium with clinopyroxene for varying melt/cpx and fluid/cpx mass fractions. Contours represent values of $D/(a^2\lambda)$. (a) Melt; (b) fluid.

hotter regions of the mantle and cross the wet solidus of peridotite, they will be incorporated into a fluid-undersaturated melt, and will impart a high activity ratio on the melt itself. Overall, our calculations indicate that diffusive effects on ($^{226}Ra/^{230}Th$) disequilibrium are important and must be included in models relating ($^{226}Ra/^{230}Th$) to magma and fluid transport rates.

7. Discussion

The calculations described above indicate that at temperatures in the range 1050–1250°C, the presence of phlogopite and/or amphibole in the mantle will mean that phlogopite, amphibole, and clinopyroxene will have steady-state ($^{226}Ra/^{230}Th$) that are different from the radioactive equilibrium values by large factors. The implications

of this condition for the $(^{226}\text{Ra}/^{230}\text{Th})$ of magma formed by partial melting of this heterogeneous solid material depend on the conditions of melt formation and extraction.

7.1. Melting of metasomatized mantle

The melting relations of phlogopite-bearing mantle are more complicated and less well studied than anhydrous mantle melting, but some aspects of the process can be inferred. Phlogopite is stable at temperatures up to 1250°C at 3.0 GPa [46–48] and 1100°C at ~ 0.1GPa [49]. Modreski and Boettcher [46] investigated the stoichiometry of the phlogopite breakdown reaction by adding excess water to synthetic mafic assemblages containing phlogopite, and found that phlogopite+diopside ± enstatite ± vapor react to form forsterite+ liquid between 1100 and 1250°C at pressures ranging from 0.5 to 3.0 GPa. In experiments run with and without excess water, nearly all the phlogopite was consumed while most of the clinopyroxene was retained. In essence, diopside behaved as a refractory phase at the onset of hydrous melting. The conclusions of Modreski and Boettcher are supported by a number of studies on similar phlogopite-bearing assemblages [48–53]. Hence at small melt fractions, it is probable that breakdown of phlogopite is the primary reaction generating liquid. If $(^{226}\text{Ra}/^{230}\text{Th})$ is high in the phlogopite, it is reasonable to believe that a melt generated by the preferential breakdown of phlogopite would likewise be enriched in ^{226}Ra over ^{230}Th. However, the degree to which a melt phase can reflect the ^{226}Ra enrichment that was originally present in the phlogopite depends on two factors: the amount that clinopyroxene contributes to the initial liquid and the rate of separation of the melt from the solid residue. Since the clinopyroxene is depleted in ^{226}Ra, any contribution to the melt from clinopyroxene will partially offset the high $(^{226}\text{Ra}/^{230}\text{Th})$ of the phlogopite. If the melt remains in contact with the solid residue after phlogopite has been exhausted from the residue, then eventually the melt phase will reach a new steady state determined by the values of $K_{\text{Ra}}^{\text{cpx/melt}}$ and $K_{\text{Th}}^{\text{cpx/melt}}$ that characterize the solid–liquid equilibrium (as in Fig. 7).

The calculated $(^{226}\text{Ra}/^{230}\text{Th})$ and Ba/Th in magma produced by melting phlogopite-bearing mantle is presented in Fig. 8a. For the calculations it is assumed that mantle lherzolite contains 10% clinopyroxene by weight, and hence for $M^{\text{cpx}}/M^{\text{phlog}}$ values of 10–1000, the modal abundance of phlogopite is about 1–0.01%. The relative contributions of phlogopite and clinopyroxene to the liquid are determined by the degree of melting. Following the experimental results of Modreski and Boettcher [46], we assume that phlogopite melts until it is exhausted, followed by clinopyroxene, which melts until it in turn is exhausted. The incongruous breakdown of orthopyroxene to olivine plus liquid is inconsequential as neither of these phases contains significant Ba, Ra, or Th. We find that the $(^{226}\text{Ra}/^{230}\text{Th})$ and Ba/Th of the melt are dependent on both $M^{\text{cpx}}/M^{\text{phlog}}$ and the melt fraction. For a given melt fraction, however, the $^{226}\text{Ra}/^{230}\text{Th}$ ratio is only marginally affected by $M^{\text{cpx}}/M^{\text{phlog}}$, due to the fact that the increasing activity ratio in the phlogopite as $M^{\text{cpx}}/M^{\text{phlog}}$ increases (Fig. 6) is offset by the decreasing contribution of phlogopite to the melt due to its lower modal abundance. When the melt fraction is equal to or less than the modal abundance of phlogopite, the melt directly reflects the isotopic and elemental composition of the phlogopite. The $(^{226}\text{Ra}/^{230}\text{Th})$ in the melt increases by roughly an order of magnitude for each order of magnitude decrease in melt fraction, and is quite large ($\gg 10$) for small melt fractions ($\sim 0.1\%$ or less).

While phlogopite has the stronger influence over Ba/Th and $(^{226}\text{Ra}/^{230}\text{Th})$ in melts of metasomatized mantle, amphibole still plays a significant role in determining (and in the absence of phlogopite may dominate) these ratios. Pargasitic amphibole has been shown to be stable to 1075°C at pressures of 1.8–2.5 GPa in MORB pyrolite [54], and up to 1150°C at 2.9 GPa in water-undersaturated Hawaiian pyrolite [38]. All of the amphibole-bearing MORB pyrolite melting experiments of Niida and Green [54] contain residual clinopyroxene in the run products, indicating that, like phlogopite, amphibole will be an early-melting phase. The activity ratios expected for melts of amphibole-bearing mantle are shown for varying Ba/Th and melt fraction in Fig. 8b.
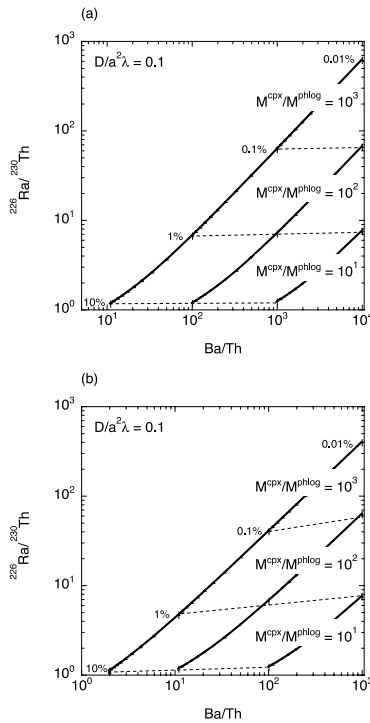
Fig. 8. (^{226}Ra/^{230}Th) vs. Ba/Th in melt generated from phlog-opite- and amphibole-bearing peridotite. Melt ratios generated by combining phlogopite or amphibole and clinopyroxene for the given values of M^{cpx}/M^{phlog} and melt fraction. Solid lines indicate M^{cpx}/M^{phlog} and dotted lines indicate varying melt percentage. Phlogopite, amphibole, and clinopyroxene (^{226}Ra/^{230}Th) is as given in Fig. 6a,c. Below the minimum melt percentage denoted for each value of M^{cpx}/M^{phlog}, the melt is essentially pure phlogopite or amphibole and the activity and concentration ratios do not vary. For all calculations, $D/(a^2\lambda) = 0.1$. (a) Phlogopite-bearing assemblage; (b) amphibole-bearing assemblage.

The correlations between (^{226}Ra/^{230}Th), Ba/Th, M^{cpx}/M^{phlog}, and melt fraction are similar to those calculated for melting a phlogopite-bearing assemblage, with the exceptions that Ba/Th is lower by about an order of magnitude and the activity ratio is slightly more dependent on M^{cpx}/M^{phlog}.

We do not treat the separation rate issue fully, but calculate instead the (^{226}Ra/^{230}Th) for the initial melt, assuming that this melt can be instantaneously separated from the residue. Because this is an end-member case, the quoted (^{226}Ra/^{230}Th) values are maxima. However, it is likely that the model melt can separate relatively quickly, be-

cause under the conditions considered, the melt will have both a high Mg content and a high water content and hence a very low viscosity. Interestingly, if the melt were unable to separate quickly, particularly in the presence of *residual* phlogopite or amphibole, fractionation may take place in the opposite sense, such that the melt may acquire (^{226}Ra/^{230}Th) < 1 due to Ra retention in the residual hydrous phases. This may be the case for some continental and ocean island alkali basalts [55,56], where the water content is lower than in arc lavas.

7.2. ^{226}Ra activity excess in arc lavas

Although moderate ^{226}Ra excesses have been measured in OIB ((^{226}Ra/^{230}Th) ≲ 1.5 [11]) and MORB ((^{226}Ra/^{230}Th) ≲ 4 [9,10]), the strongest excesses measured to date have been in island arc lavas ((^{226}Ra/^{230}Th) ≲ 8 [7,8])(Fig. 1). The highest (^{226}Ra/^{230}Th) is found in the most primitive arc lavas [8], indicating a mantle source for high (^{226}Ra/^{230}Th) lavas. As Ra is fluid-soluble, while Th is not, it may be reasonable to assume that high (^{226}Ra/^{230}Th) could be the result of fluid interaction in the mantle wedge. Correlations between (^{226}Ra/^{230}Th) and (^{238}U/^{230}Th), Ba/Th [8], and ^{10}Be/Be [15] have been noted in arcs worldwide, suggesting that these enrichments may be due to the addition of a single component, namely a slab-derived fluid.

The idea that U-series disequilibria are imparted by a single fluid interaction, however, is contradicted by the time scales given by the different isochrons. Large radium activity excesses cannot persist for more than 8000 yr, while (^{238}U/^{230}Th) and (^{231}Pa/^{235}U) isochrons yield fluid addition ages of ∼ 60 ka for the Tonga–Kermadec Arc [12,17] and ∼ 30 ka for the Mariana arc [57]. Establishing a means by which enrichment events seemingly separated by tens of thousands of years could be correlated is difficult. One appealing explanation involves a distillation of the fluid, in which the first fluid released from the slab contains all of the U but leaves behind the Th, and later fluids contain only Ra that has grown in from Th, but no U [12]. However, it is unlikely that reality is so straightforward. For instance,

the simplicity of this model is contra-indicated by the persistence of garnet in the eclogitic residue, which suggests that considerable U is retained following the initial slab dehydration [28].

We propose that the $(^{230}Th/^{238}U)$ and $(^{226}Ra/^{230}Th)$ disequilibria in arc lavas are the result of a continuous dehydration process, but whereas the $(^{230}Th/^{238}U)$ records the age of the initial slab dehydration, the $(^{226}Ra/^{230}Th)$ develops subsequently in the mantle wedge by the diffusion process described above. Water-rich fluid generated by dehydration reactions in the down-going slab migrates into the mantle wedge and crystallizes phlogopite and amphibole, resulting in a modally metasomatized peridotite mantle [19,20,58]. Uranium and thorium are fractionated by slab dehydration processes [5], but not phlogopite or amphibole crystallization [27–29], and both diffuse slowly in clinopyroxene [36]. Consequently, the measured $(^{230}Th/^{238}U)$ in arc lavas reflects the original fractionation associated with slab dehydration, modified only by radioactive decay. It takes only a few thousand years for $(^{226}Ra/^{230}Th)$ steady-state disequilibrium to develop in the minerals of the metasomatized mantle wedge, and this isotopic signature is permanently available to be imparted on small-degree melts. Therefore both $(^{230}Th/^{238}U)$ and $(^{226}Ra/^{230}Th)$ disequilibria are produced by the same fluid transfer event, but by different mechanisms, and at the time of melting, the $(^{230}Th/^{238}U)$ effect has partially decayed away but the $(^{226}Ra/^{230}Th)$ effect has not. The correlation of $(^{226}Ra/^{230}Th)$ with $(^{230}Th/^{238}U)$, Ba/Th and $^{10}Be/Be$ is due to the high ratios of these elements/isotopes in slab-derived fluids and preserved by their relative compatibility in phlogopite and amphibole [27,28,59].

Alternatively, it has been suggested that $(^{230}Th/^{238}U)$, $(^{226}Ra/^{230}Th)$, and $(^{231}Pa/^{235}U)$ correlations are determined by fluxing the mantle with a fluid component enriched in Ra and U, but also carrying some Pa and Th, and thus do not yield true isochrons at all [18]. Similar results are obtained by mixing an enriched melt generated by phlogopite breakdown with a variably depleted, larger volume mantle melt. The two magma end-members originate as a result of phlogopite and/or amphibole crystallization from slab-derived fluids

or hydrous melts. If the hydrous minerals are not able to accommodate all of the H_2O, the excess fluid can separate and migrate into the mantle above [20]. Ultimately, the separated fluid induces wet mantle melting, which provides the larger-degree (depleted) melt. Alternatively, the large-degree melt could be generated by decompression melting in the mantle wedge [60]. The hydrous solid phases also migrate into warmer regions of the mantle, albeit on a slower time scale, where they melt to form the enriched component. Magma generated by mixing 1–10% ^{226}Ra-enriched contaminant with 90–99% variably depleted magma at secular equilibrium is depicted in Fig. 9, with lavas from the Tonga–Kermadec Arc [12,17] shown for comparison. We have allowed the degree of depletion in the larger melt to vary over a limited range (i.e. [Th] = 0.1–1 ppm, [Ba] and [Ra] vary proportionally to [Th]), due to the degree of melting and/or prior depletion in the back-arc. The higher the concentrations of Ba, Ra, and Th, the less the composition of the magma is affected by the addition of the phlogopite/amphibole component, resulting in the observed correlations. The trend shown in Fig. 9b can also be successfully, and perhaps more simply, explained by decreasing $(^{226}Ra/^{230}Th)$ as magma differentiation proceeds through time [12]. However, it may be difficult to achieve the range of Ba/Th ratios in Fig. 9a by differentiation alone.

The phenomenon described above might also be accomplished by aqueous fluids themselves, without the intervening hydrous mineral phase. The mobility of a fluid in the mantle is determined by the dihedral angle at the triple junctions between mineral grains. If the dihedral angle is greater than 60°, fluid is held in isolated pockets at the grain boundaries. If the dihedral angle is less than 60°, the fluid forms an interconnected network and is thereby mobile. Mibe et al. [61] show that the dihedral angle of forsterite is greater than 60° at the pressure and temperature conditions of dehydration in the subducted slab, but less than 60° at higher temperatures and pressures. Therefore, a fluid released during slab dehydration could be trapped at grain boundaries and dragged along with the descending slab until it reaches the right conditions for fluid mobiliza-
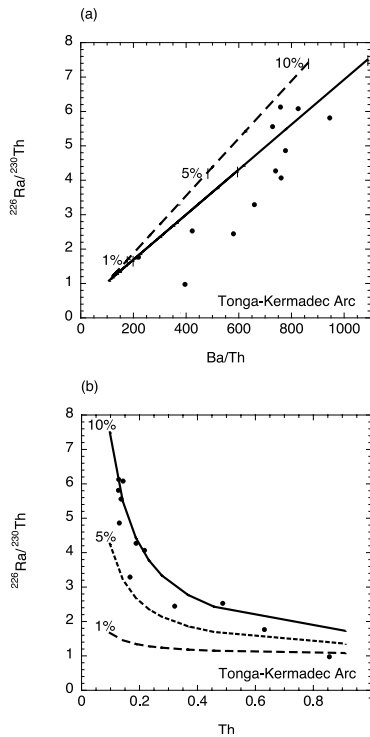
Fig. 9. (a) $(^{226}Ra/^{230}Th)$ vs. Ba/Th in magma generated by mixing 1–10% ^{226}Ra-enriched, low-degree melt with 90–99% variably depleted, high-degree melt that is at secular equilibrium. Solid line represents the calculated mixing line where the enriched end-member is pure phlogopite melt, and dashed line represents mixing line for enriched end-member composed of 3:1 phlogopite:amphibole. Ticks denote the percentage of enriched end-member contribution to the mix. $(^{226}Ra/^{230}Th)$ and Ba/Th in enriched end-member from Fig. 8, where melt percentage is 0.1%, $M^{cpx}/M^{phlog(amph)} = 100$, and $D/(a^2\lambda) = 0.1$. We assume that Ba/Th = 100 in the depleted melt, 10^4 in the phlogopite melt, and 10^3 in the amphibole melt. Tonga–Kermadec Arc data from [8,14]. (b) $(^{226}Ra/^{230}Th)$ vs. Th. The Th concentration in the high-degree melt varies from 0.1 to 1 ppm, while the Th concentration in the low-degree melt is always 0.1 ppm. Solid and dashed lines represent the addition of 1%, 5%, and 10% high-Ra melt to the larger melt.

tion. During this time, $(^{226}Ra/^{230}Th)$ disequilibrium could grow into the fluid by diffusion, as shown in Fig. 7b, while $(^{238}U/^{230}Th)$ simply evolves toward equilibrium. Once mobilized, this fluid could contribute its unique isotopic and trace element characteristics to melt generated in the mantle above.

7.3. Time constraints for melt transport

The very existence of ^{226}Ra excesses in lavas sampled at the surface implies that these magmas migrate from the source area to the surface quickly. In ca. 8000 yr (five half-lives or about three mean lives), the magmas will have returned to secular equilibrium, and after only 1600 yr, the ^{226}Ra activity will have decreased by one-half. The very large ^{226}Ra excesses observed in some arc lavas have led researchers to propose 'ultra-fast' magma migration, on the order of 1000 m/yr [8], such that magma can move from subduction zone to surface in about 100 yr. This high transport rate is about two orders of magnitude faster than predicted by physical models for rapid melt migration [62].

Part of the reason for the inferred high melt migration velocities is that the standard models for the generation of $(^{226}Ra/^{230}Th)$ disequilibrium in magmas involve fractionation of Ra from Th by partial melting starting with a solid assemblage where all of the minerals are at secular equilibrium. In such a model, Ra/Th fractionation is limited by the differences in melt/solid partitioning between the two elements, and activity ratios as high as 8 may be difficult to generate at all. The direct addition of an aqueous fluid can increase the $(^{226}Ra/^{230}Th)$, but this effect is largely unconstrained and difficult to reconcile with the multiple time scales of U-series fractionation in arcs. We argue, however, that if mantle metasomatism is prevalent throughout the mantle wedge, and solid state mineral disequilibrium characterizes the mantle, then magmas may start out with higher $(^{226}Ra/^{230}Th)$, and incipient non-equilibrium melting of metasomatic minerals along channel walls could serve to maintain ^{226}Ra excesses during migration. In fact, it is possible that the $(^{226}Ra/^{230}Th)$ enrichment may not originate deep in the mantle at all. Some alkali basalts contain megacrysts of phlogopite and amphibole, presumably acquired from hydrous veins in the upper mantle shortly prior to or during eruption [63]. Phlogopite–pyroxenite diapirs, originating from the slab–wedge interface and rising to accumulate at the base of the crust [20], would also provide the necessary mineral assemblage for sol-

id-state Ra diffusion, hence (^{226}Ra/^{230}Th) disequilibrium, provided that the temperature is high enough. If the phlogopite were assimilated shortly prior to eruption, the increased (^{226}Ra/^{230}Th) of the melt might not reflect migration time from the source at all, but rather shallow level contamination.

7.4. Application to other U-series isotopes

Other U-series isotope ratios could be affected by the process described here. The general requirements are that the parent and daughter nuclides be fractionated significantly by different mineral phases, and that the diffusion parameter for the daughter nuclide $D_i/a^2\lambda_i$ be sufficiently large to allow diffusive redistribution to occur. For the range of grain sizes and temperatures applicable to subduction zone environments, (^{226}Ra/^{230}Th) disequilibrium is the only effect likely to be of significant magnitude if the fractionating phase is phlogopite or amphibole. However, for smaller grain sizes and higher temperatures, it may be possible to generate some effect on (^{230}Th/^{238}U), and potentially (^{231}Pa/^{235}U), for instance. If the fractionating phase is an aqueous fluid, the (^{226}Ra/^{230}Th) disequilibrium is likely to be accompanied by (^{230}Th/^{238}U) disequilibrium due to the greater solubility of U in aqueous fluids.

8. Conclusions

We have shown that steady-state (^{226}Ra/^{230}Th) disequilibrium can be maintained in individual mineral phases constituting a metasomatized mantle assemblage. Since Ra is both incompatible and has a high diffusion coefficient in clinopyroxene, ^{226}Ra generated by the decay of ^{230}Th diffuses out of the clinopyroxene and into neighboring phases where it is more compatible. The result is steady-state ^{226}Ra depletion in clinopyroxene and enrichment in phases such as phlogopite and amphibole. The relative contributions of these mantle minerals to a melt determine its initial (^{226}Ra/^{230}Th) signature. As U and Th both diffuse very slowly in clinopyroxene, and are more evenly distributed among the relevant phases at equilibrium, U and Th are less likely to be fractionated by the same mechanism in subduction zones.

Although ^{226}Ra enrichment in island arcs is indirectly the result of fluid addition to the mantle, and therefore correlated with other geochemical indicators of fluid addition, ^{226}Ra-^{230}Th does not record the time of fluid addition, but rather the time of melting. The storage of U and Th in phlogopite or amphibole, as opposed to the diffusive addition of Ra to these phases, leads to the unusual situation whereby these two U-series systems, while correlated in magnitude, are decoupled in time. Partial melting of hydrous minerals at shallow levels can obscure information regarding melt generation and transport times that might otherwise be obtained from (^{226}Ra/^{230}Th) disequilibria.

References

[1] D. McKenzie, The extraction of magma from the crust and mantle, Earth Planet. Sci. Lett. 74 (1985) 81–91.

[2] P.D. Beattie, Uranium-thorium disequilibria and partitioning on melting of garnet peridotite, Nature 363 (1993) 63–65.

[3] M. Spiegelman, T. Elliott, Consequences of melt transport for uranium series disequilibrium in young lavas, Earth Planet. Sci. Lett. 118 (1993) 1–20.

[4] C. Lundstrom, J. Gill, Q. Williams, A geochemically consistent hypothesis for MORB generation, Chem. Geol. 162 (2000) 105–126.

[5] J. Gill, R. Williams, Th isotope and U-series studies of subduction-related volcanic rocks, Geochim. Cosmochim. Acta 54 (1990) 1427–1442.

[6] M. Reagan, J. Morris, E. Herrstrom, M. Murrell, Uranium series and beryllium isotope evidence for an extended history of subduction modification of the mantle below Nicaragua, Geochim. Cosmochim. Acta 58 (1994) 4199–4212.

[7] J. Hoogewerff, M. van Bergen, P. Vroon, J. Hertogen, R. Wordel, A. Sneyers, A. Nasution, J. Varekamp, H. Moens, D. Mouchel, U-series, Sr-Nd-Pb isotope and trace-element systematics across an active island arc-continent collision zone: Implications for element transfer at the slab-wedge interface, Geochim. Cosmochim. Acta 61 (1997) 1057–1072.

[8] S. Turner, P. Evans, C.J. Hawkesworth, Ultrafast source-to-surface movement of melt at island arcs from ^{226}Ra-^{230}Th systematics, Science 292 (2001) 1363–1366.

[9] C. Lundstrom, D. Sampson, M. Perfit, J. Gill, Q. Williams, Insights into mid-ocean ridge basalt petrogenesis: U-series disequilibria from the Siqueiros Transform, Lamont Seamounts, and East Pacific Rise, J. Geophys. Res. 104 (1999) 13035–13048.

[10] K.W. Sims, S.J. Goldstein, J. Blichert-Toft, M. Perfit, P. Kelemen, D.J. Fornari, P. Michael, M.T. Murrell, S.R. Hart, D.J. DePaolo, G. Layne, L. Ball, M. Jull, J. Bender, Chemical and isotopic constraints on the generation and transport of magma beneath the East Pacific Rise, Geochim. Cosmochim. Acta 66 (2002) 3481–3504.

[11] K.W. Sims, D.J. DePaolo, M.T. Murrell, W.S. Baldridge, S. Goldstein, D. Clague, M. Jull, Porosity of melting zone and variations in the solid mantle upwelling rate beneath Hawaii: Inferences from ^{238}U-^{230}Th-^{226}Ra and ^{235}U-^{231}Pa disequilibria, Geochim. Cosmochim. Acta 63 (1999) 4119–4138.

[12] S. Turner, B. Bourdon, C. Hawkesworth, P. Evans, ^{226}Ra-^{230}Th evidence for multiple dehydration events, rapid melt ascent and the time scales of differentiation beneath the Tonga-Kermadec island arc, Earth Planet. Sci. Lett. 179 (2000) 581–593.

[13] K.M. Cooper, M.R. Reid, M.T. Murrell, D.A. Clague, Crystal and magma residence at Kilauea Volcano, Hawaii: ^{230}Th-^{226}Ra dating of the 1955 east rift eruption, Earth Planet. Sci. Lett. 184 (2001) 703–718.

[14] S. Turner, J. Foden, U, Th, and Ra disequilibria, Sr, Nd, and Pb isotope and trace element variations in Sunda Arc lavas: predominanace of a subducted sediment component, Contrib. Mineral. Petrol. 142 (2001) 43–57.

[15] O. Sigmarsson, J. Chmeleff, J. Morris, L. Lopez-Escobar, Origin of ^{226}Ra-^{230}Th disequilibria in arc lavas from southern Chile and implications for magma transfer time, Earth Planet. Sci. Lett. 196 (2002) 189–196.

[16] S.K. Clark, M.K. Reagan, T. Plank, Trace element and U-series systematics for 1963-1965 tephras from Irazu Volcano, Costa Rica: implications for magma generation processes and transit times, Geochim. Cosmochim. Acta 62 (1998) 2689–2699.

[17] S. Turner, C. Hawkesworth, N. Rogers, J. Bartlett, T. Worthington, J. Hergt, J. Pearce, I. Smith, ^{238}U-^{230}Th disequilibria, magmatic petrogenesis, and flux rates beneath the depleted Tonga-Kermadec island arc, Geochim. Cosmochim. Acta 61 (1997) 4855–4884.

[18] R.B. Thomas, M.M. Hirschmann, H. Cheng, M.K. Reagan, R.L. Edwards, (^{231}Pa/^{235}U)-(^{230}Th/^{238}U) of young mafic volcanic rocks from Nicaragua and Costa Rica and the influence of flux melting on U-series systematics of arc lavas, Geochim. Cosmochim. Acta 66 (2002) 4287–4309.

[19] J.H. Davies, D.J. Stevenson, Physical model of source region of subduction zone volcanics, J. Geophys. Res. 97 (1992) 2037–2070.

[20] P. Wyllie, T. Sekine, The formation of mantle phlogopite in subduction zone hybridization, Contrib. Mineral. Petrol. 79 (1982) 375–380.

[21] A. Zanetti, M. Mazzucchelli, G. Rivalenti, R. Vannucci, The Finero phlogopite-peridotite massif: an example of subduction-related metasomatism, Contrib. Mineral. Petrol. 134 (1999) 107–122.

[22] D. Ionov, A. Hofmann, Nb-Ta-rich mantle amphiboles and micas: Implications for subduction-related metasomatic trace element fractionations, Earth Planet. Sci. Lett. 131 (1995) 341–356.

[23] D. Ionov, W. Griffin, S. O'Reilly, Volatile-bearing minerals and lithophile trace elements in the upper mantle, Chem. Geol. 141 (1997) 153–184.

[24] S. O'Reilly, W. Griffin, C. Ryan, Residence of trace elements in metasomatized spinel lherzolite xenoliths: a proton-microprobe study, Contrib. Mineral. Petrol. 109 (1991) 98–113.

[25] B. Moine, J-Y. Cottin, S. Sheppard, M. Gregoire, S. O'Reilly, A. Giret, Incompatible trace element and isotopic (D/H) characteristics of amphibole- and phlogopite-bearing ultramafic to mafic xenoliths from Kerguelen Islands (TAAF, South Indian Ocean), Eur. J. Mineral. 12 (2000) 761–777.

[26] R.D. Shannon, Revised effective ionic radii and systematic studies of interatomic distances in halides and chalcogenides, Acta Cryst. 32 (1976) 751–767.

[27] M.D. Feineman, D.J. DePaolo, F.J. Ryerson, I.D. Hutcheon, Mica-aqueous fluid partitioning of trace elements at upper mantle conditions: Implications for the chemistry of slab-derived fluids, EOS Trans. AGU 81 (48), Fall Meet. Suppl., Abstract V21G-06 (2000).

[28] J. Brenan, H. Shaw, F. Ryerson, D. Phinney, Mineral-aqueous fluid partitioning of trace elements at 900°C and 2.0 GPa: Constraints on the trace element chemistry of mantle and deep crustal fluids, Geochim. Cosmochim. Acta 59 (1995) 3331–3350.

[29] T. LaTourrette, R. Hervig, J. Holloway, Trace element partitioning between amphibole, phlogopite, and basanite melt, Earth Planet. Sci. Lett. 135 (1995) 13–30.

[30] E.H. Hauri, T.P. Wagner, T.L. Grove, Experimental and natural partitioning of Th, U, Pb, and other trace elements between garnet, clinopyroxene, and basaltic melts, Chem. Geol. 117 (1994) 149–166.

[31] S. Foley, S. Jackson, B. Fryer, J. Greenough, G. Jenner, Trace element partition coefficients for clinopyroxene and phlogopite in an alkaline lamprophyre from Newfoundland by LAM-ICP-MS, Geochim. Cosmochim. Acta 60 (1996) 629–638.

[32] J.D. Blundy, B.J. Wood, Prediction of crystal-melt partition coefficients from elastic moduli, Nature 372 (1994) 452–454.

[33] B.J. Wood, J.D. Blundy, A predictive model for rare earth element partitioning between clinopyroxene and anhydrous silicate melt, Contrib. Mineral. Petrol. 129 (1997) 166–181.

[34] J.C. Brice, Some thermodynamic aspects of the growth of strained crystals, J. Cryst. Growth 28 (1975) 249–253.

[35] J. Blundy, B. Wood, Mineral-melt partitioning of uranium, thorium, and their daughters, in: B. Bourdon, G.M. Henderson, C.C. Lundstrom, S.P. Turner (Eds.), Uranium Series Geochemistry, Rev. Mineral. Geochem. 52, Mineral. Soc. Am., Washington, DC, 2003, pp. 59–118.

[36] J.A. VanOrman, T.L. Grove, N. Shimizu, Uranium and thorium diffusion in diopside, Earth Planet. Sci. Lett. 160 (1998) 505–519.

[37] J.A. Van Orman, T.L. Grove, N. Shimizu, Rare earth element diffusion in diopside: influence of temperature, pressure, and ionic radius, and an elastic model for diffusion in silicates, Contrib. Mineral. Petrol. 141 (2001) 687–703.

[38] K.M. Cooper, Time scales of magma generation, differentiation, and storage: constraints from uranium-238-thorium-230-radium-226 disequilibria, PhD Thesis, University of California Los Angeles (2001).

[39] J. Farver, R. Yund, Grain boundary diffusion of oxygen, potassium, and calcium in natural and hot-pressed feldspar aggregates, Contrib. Mineral. Petrol. 118 (1995) 340–355.

[40] M. Sneeringer, S. Hart, N. Shimizu, Strontium and samarium diffusion in diopside, Geochim. Cosmochim. Acta 48 (1984) 1589–1608.

[41] B. Giletti, G. Layne, Diffusion of Sr in biotite and F-phlogopite micas, EOS Trans. AGU 80 (46), Fall Meet. Suppl., Abstract V51B-1015 (2001).

[42] D.J. Cherniak, Pb diffusion in Cr diopside, augite, enstatite, and consideration of the dependence of cation diffusion in pyroxene on oxygen fugacity, Chem. Geol. 177 (2001) 381–397.

[43] H. Iwamori, ^{238}U-^{230}Th-^{226}Ra and ^{235}U-^{231}Pa disequilibria produced by mantle melting with porous and channel flows, Earth Planet. Sci. Lett. 125 (1994) 1–16.

[44] Z. Qin, Disequilibrium partial melting model and its implications for trace element fractionations during mantle melting, Earth Planet. Sci. Lett. 112 (1992) 75–90.

[45] M. Jull, P. Kelemen, K. Sims, Consequences of diffuse and channeled porous melt migration on uranium series

disequilibria, Geochim. Cosmochim. Acta 66 (2002) 4133–4148.

[46] P.J. Modreski, A.L. Boettcher, Phase relationships of phlogopite in the system K_2O-MgO-CaO-Al_2O_3-SiO_2-H_2O to 35 kilobars: a better model for micas in the interior of the earth, Am. J. Sci. 273 (1973) 385–414.

[47] J.R. Holloway, D.H. Eggler, Fluid-absent melting of peridotite containing phlogopite and dolomite, Carnegie Inst. Washington Yearb. 75 (1976) 636–639.

[48] R.F. Wendlandt, D.H. Eggler, The origins of potassic magmas: stability of phlogopite in natural spinel lherzolite and in the system $KAlSiO_4$-MgO-SiO_2-H_2O-CO_2 at high pressures and high temperatures, Am. J. Sci. 280 (1980) 421–458.

[49] K. Righter, I.S.E. Carmichael, Phase equilibria of phlogopite lamprophyres from western Mexico: biotite-liquid equilibria and P-T estimates for biotite-bearing igneous rocks, Contrib. Mineral. Petrol. 123 (1996) 1–21.

[50] P.J. Modreski, A.L. Boettcher, The stability of phlogopite and enstatite at high pressures: a model for micas in the interior of the earth, Am. J. Sci. 272 (1972) 852–869.

[51] T. Sekine, P. Wyllie, Phase relationships in the system $KAlSiO_4$-Mg_2SiO_4-SiO_2-H_2O as a model for hybridization between hydrous siliceous melts and peridotite, Contrib. Mineral. Petrol. 79 (1982) 368–374.

[52] D.H. Green, Experimental melting studies on a model upper mantle composition at high pressure under water-undersaturated conditions, Earth Planet. Sci. Lett. 19 (1973) 37–53.

[53] S. Esperança, J. Holloway, On the origin of some mica-lamprophyres: experimental evidence from a mafic minette, Contrib. Mineral. Petrol. 95 (1987) 207–216.

[54] K. Niida, D.H. Green, Stability and chemical composition of pargasitic amphibole in MORB pyrolite under upper mantle conditions, Contrib. Mineral. Petrol. 135 (1999) 18–40.

[55] R. Williams, J. Gill, Th isotopes and U-series disequilibria in some alkali basalts, Geophys. Res. Lett. 19 (1992) 139–142.

[56] C. Claude-Ivanaj, J-L. Joron, C. Allègre, ^{238}U-^{230}Th-^{226}Ra fractionation in historical lavas from the Azores: long-lived source heterogeneity vs. metasomatism fingerprints, Chem. Geol. 176 (2001) 295–310.

[57] T. Elliott, T. Plank, A. Zindler, W. White, B. Bourdon, Element transport from slab to volcanic front at the Mariana arc, J. Geophys. Res. 102 (1997) 14991–15019.

[58] G. Prouteau, B. Scaillet, M. Pichavant, R. Maury, Evidence for mantle metasomatism by hydrous silicic melts derived from subducted oceanic crust, Nature 410 (2001) 197–200.

[59] J.M. Brenan, F.J. Ryerson, H.F. Shaw, The role of aqueous fluids in the slab-to-mantle transfer of boron, beryllium, and lithium during subduction: experiments and models, Geochim. Cosmochim. Acta 62 (1998) 3337–3347.

[60] T.L. Grove, S.W. Parman, S.A. Bowring, R.C. Price, M.B. Baker, The role of an H_2O-rich fluid component

in the generation of primitive basaltic andesites and andesites from the Mt. Shasta region, N California, Contrib. Mineral. Petrol. 142 (2002) 375–396.

[61] K. Mibe, T. Fujii, A. Yasuda, Control on the location of the volcanic front in island arcs by aqueous fluid connectivity in the mantle wedge, Nature 401 (1999) 259–261.

[62] P.S. Hall, C. Kincaid, Diapiric flow at subduction zones: a recipe for rapid transport, Science 292 (2001) 2472–2475.

[63] K. Righter, I.S.E. Carmichael, Mega-xenocrysts in alkali olivine basalts: Fragments of disrupted mantle assemblages, Am. Mineral. 78 (1993) 1230–1245.